

1 **Estimating terrestrial gross primary productivity in water limited**  
2 **ecosystems across Africa using the Southampton Carbon Flux (SCARF)**

3 **Model**

4 P. Chiwara<sup>1, 2</sup>, B.O. Ogutu<sup>1\*</sup>, J. Dash<sup>1</sup>, E.J. Milton<sup>1</sup>, J. Ardo<sup>3</sup>, M. Saunders<sup>4</sup> and G.  
5 Nicolini<sup>5</sup>

6 1: Dept. of Geography and Environment, University of Southampton, United  
7 Kingdom;

8 2: Dept. of Geography and Population Studies, Lupane State University,  
9 Bulawayo, Zimbabwe;

10 3: Dept. of Physical Geography and Ecosystem Science, Lund University, Sweden;

11 4: Dept. of Botany, School of Natural Sciences, Trinity College Dublin, Ireland;

12 5: Euro-Mediterranean Center on Climate Change (CMCC), Trieste, Italy

13 **\*Corresponding author:** Email boo1c14@soton.ac.uk

14

15 **Abstract**

16 The amount of carbon uptake by vegetation is an important component to  
17 understand the functioning of ecosystem processes and their response/feedback  
18 to climate. Recently, a new diagnostic model called the Southampton Carbon Flux  
19 (SCARF) Model driven by remote sensing data was developed to predict terrestrial  
20 gross primary productivity (GPP) and successfully applied in temperate regions.

21 The model is based on the concept of quantum yield of plants and improves on  
22 the previous diagnostic models by (i) using the fraction of photosynthetic active  
23 radiation absorbed by the photosynthetic pigment (FAPAR<sub>ps</sub>) and (ii) using direct

24 quantum yield by classifying the vegetation into C<sub>3</sub> or C<sub>4</sub> classes. In this paper,  
25 we calibrated and applied the model to evaluate GPP across various ecosystems  
26 in Africa. The performance of the model was evaluated using data from seven  
27 eddy covariance flux tower sites. Overall, the modelled GPP values showed good  
28 correlation ( $R > 0.59$ ,  $p < 0.0001$ ) with estimated flux tower GPP at most sites  
29 (except at a tropical rainforest site,  $R = 0.38$ ,  $p = 0.02$ ) in terms of their  
30 seasonality and absolute values. Mean daily GPP across the investigated period  
31 varied significantly across sites depending on the vegetation types from a  
32 minimum of  $0.44 \text{ gC m}^{-2} \text{ day}^{-1}$  at the semi-arid and sub-humid savanna grassland  
33 sites to a maximum of  $9.86 \text{ gC m}^{-2} \text{ day}^{-1}$  at the woodland and tropical rain forest  
34 sites. Generally, strong correlation is observed in savanna woodlands and  
35 grasslands where vegetation follows a prescribed seasonal cycle as determined by  
36 changes in canopy chlorophyll content and leaf area index. Finally, the mean  
37 annual GPP value for Africa predicted by the model was  $35.25 \text{ Pg C yr}^{-1}$ . The good  
38 performance of the SCARF model in water-limited ecosystems across Africa  
39 extends its potential for global application.

40

41 **Key words:** Gross primary productivity, remote sensing, diagnostic model,  
42 carbon exchange, photosynthetic quantum yield, C<sub>3</sub>/C<sub>4</sub> photosynthesis

43

44

45

46

47

48 **1. Introduction**

49 Gross primary productivity (GPP) plays a critical role in the functioning of  
50 terrestrial ecosystems particularly through the regulation of water, energy and  
51 nutrient cycles (Gitelson et al., 2012; Verma et al., 2005). While there has been  
52 significant improvements in reliability of the estimates of terrestrial GPP in other  
53 regions of the world, particularly North America and Europe, estimates remain  
54 highly uncertain across the African continent (Ardo et al., 2008; Merbold et al.,  
55 2009; Papale et al., 2006; Sjöström et al., 2011). This is despite wide  
56 acknowledgement about the critical contributions made by the continent's  
57 ecosystems in global carbon dynamics (e.g. Ciais et al., 2011; Sjöström et al.,  
58 2011). For example, estimates by Williams et al. (2007) indicated that ecosystems  
59 across Africa account for as much as one-fifth of global GPP which is mainly  
60 attributed to vastness of the tropical rainforests and the savanna ecosystems.  
61 Although recent estimates place Africa as carbon neutral (e.g. Williams et al.,  
62 2007), rapid population growth and urbanization (Birch & Wachter, 2011) and  
63 general improvement in standards of living (Potts, 2012) are likely to worsen the  
64 continent's heavy dependency on natural resources causing uncertainties to its  
65 future carbon balance. The uniqueness of African ecosystems is also marked by  
66 the heterogeneous nature of the savanna ecosystems which poses challenges in  
67 allocating light conversion efficiencies in global GPP models (Suyker & Verma,  
68 2010, 2012).

69 The uncertain nature of current CO<sub>2</sub> fluxes demands that efforts are directed  
70 towards improving data and knowledge availability if we are to improve on future  
71 predictions for this region. Several projects have been established as part of  
72 initiatives to improve data availability on greenhouse gas (GHG) fluxes for Africa,

73 for example the CARBOAFRICA Project which set up the first flux network for Africa  
74 in 2006 (Baldochi et al., 2012; Papale et al., 2006; Sjöström et al., 2011).  
75 Although the EC technique remains an efficient source of consistent estimation of  
76 ecosystem GPP at local scale (Falge et al., 2002; McCallum et al., 2013; Wu et al.,  
77 2010, Ran et al., 2016), the reliability of the estimates are limited only to the  
78 extent of the tower footprint in operation. This renders it impractical for estimating  
79 carbon fluxes at regional scale especially given the limited spatial coverage of flux  
80 sites across the continent (Ardo et al., 2008).

81 Many models with varying assumptions on how ecosystems respond to  
82 environmental factors have been developed for scaling up EC measurements and  
83 provide a detailed spatial temporal variation of GPP at a regional to global scale  
84 (Coops et al., 2009). In particular, the production efficiency group of models (PEM)  
85 (e.g. Ruimy et al, 1999; Turner et al., 2003; Veroustraete et al, 2002) which are  
86 based on the light use efficiency concept (LUE) (Monteith, 1972) has been widely  
87 adopted. The LUE concept suggests that ecosystem GPP is a function of the  
88 amount of photosynthetically active radiation (PAR) intercepted by a canopy,  
89 fraction of PAR that is actually absorbed by the canopy (FAPAR) and interacting  
90 environmental stress factors that tend to limit potential maximum efficiency  
91 (Monteith, 1972). The growth in the use of this family of models is largely due to  
92 the ever-increasing available knowledge, data and techniques to derive its key  
93 driving variables from Earth Observation (EO) data (Verma et al., 2005, Hilker et  
94 al., 2008).

95 Even though the inception of EO has significantly contributed to advancements in  
96 carbon flux modelling, results are still uncertain. An inter-comparison of global  
97 models (including both diagnostic and prognostic models) by Cramer et al. (1999)

98 indicate considerable uncertainty in estimated GPP (a range of 44.4 PgCyr<sup>-1</sup> to  
99 66.3 PgCyr<sup>-1</sup>) across seventeen participating models. A recent review of GPP  
100 spatial-temporal patterns by Anav et al (2015) also found large variations in global  
101 mean GPP estimates from various models. In a separate study, Williams et al.  
102 (2007) documented that although the level of error from many global models is  
103 varied, most seem to concur that as much as 50% of the uncertainty is attributed  
104 to the African ecosystems. Such variations could arise since different models adopt  
105 different assumptions to simulate ecosystem structure and vegetation responses  
106 to complex interactions of environmental factors (Gitelson et al., 2012). For  
107 example, most PEMs (e.g. MOD17 Product) use a constant maximum LUE to  
108 represent a given biome. This results in reduced ability of the models to capture  
109 species-specific LUE variations between plant functional types (PFTs), across  
110 seasons, as well as across plant development stages.

111 The ability to infer vegetation condition and structure from space-borne  
112 measurements makes it possible to derive FAPAR from satellite based indices like  
113 the normalised difference vegetation index (NDVI) (Asrar et al., 1992; Fensholt et  
114 al., 2004; Ogutu and Dash, 2013) and leaf area index (LAI) (Jarvis & Leverenz,  
115 1983, Li et al., 2015). The accurate estimation of FAPAR is important for reliable  
116 GPP estimates since FAPAR indicates the level of light absorption in the integrated  
117 canopy and consequently controls plant physiological processes represented in  
118 productivity models (Myneni & Williams, 1994; Ruimy et al., 1999). Recent studies  
119 have also indicated that the use of whole canopy FAPAR (FAPAR<sub>ca</sub>) to estimate  
120 GPP, as it is often the case with PEM models, tends to propagate uncertainty as  
121 FAPAR<sub>ca</sub> includes light absorbed by non-photosynthesizing components of the  
122 canopy e.g. stem, tree branches and dead foliage (Ogutu & Dash, 2013; Zhang et

123 al., 2014; Zhang et al., 2012; Zhang et al., 2009; Zhang et al., 2016). Ogotu &  
124 Dash (2013) gave a clear distinction between FAPAR for the whole canopy and the  
125 actual photosynthetic FAPAR (FAPAR<sub>ps</sub>) based on an inverted relationship between  
126 net ecosystem exchange (NEE) and incoming PAR. Their results concluded that  
127 the FAPAR for whole canopy is consistently higher than that actually used for  
128 photosynthesis suggesting that the use of the former may result in an  
129 overestimation of GPP and the amount of this overestimation may vary across the  
130 growing season. Additional errors in the PEMs may emanate from the use of coarse  
131 resolution land cover maps and meteorological data and thus lead to  
132 inconsistencies in the estimates of the LUE term (Harris & Dash, 2010; Sims et  
133 al., 2006; Wu et al., 2009, Ran et al., 2016).

134 Recently, a new model called Southampton Carbon Flux Model (SCARF, Ogotu et  
135 al., 2013) was developed with the aim of mitigating some of the above  
136 shortcomings. For example, it uses the fraction of PAR absorbed only by the  
137 photosynthetic components of the canopy (FAPAR<sub>ps</sub>) derived from a spectral index  
138 that is sensitive to canopy chlorophyll content for a wide range of vegetation  
139 canopies (i.e. the MERIS terrestrial chlorophyll index - MTCI, Dash & Curran,  
140 2004). In addition, the model exploits the intrinsic quantum yield of the two main  
141 photosynthetic pathways of plants (C3 and C4 photosynthesis) and does not  
142 primarily depend on a detailed land cover map to determine the ability of different  
143 vegetation species to convert light energy into biomass. The initial evaluation of  
144 the model in ecosystems where vegetation development is mainly controlled by  
145 temperature (e.g. Northern higher latitudes) showed good agreement with *in-situ*  
146 measurements (Ogotu et al., 2013).

147 In this study, we calibrated this model and used it to estimate GPP in ecosystems  
148 across Africa, where moisture is the main determinant of ecosystem GPP (Scholes  
149 et al., 2004; Svoray & Karnieli, 2011; Weber et al., 2009). Apart from evaluating  
150 the models performance in relation to *in-situ* GPP measurements and MOD17 GPP  
151 product, the study also investigated the sensitivity and uncertainty of the SCARF  
152 model to determine the relative importance of the main biophysical and  
153 meteorological input parameters to the model's output.

154

## 155 **2. Data and methods**

### 156 **2.1. The SCARF model**

157 The SCARF Model follows the general form of PEM models but it has extended  
158 capability by separating  $FAPAR_{ps}$  from  $FAPAR_{ca}$ . The LUE term is also replaced by  
159 an intrinsic quantum yield term that specifies the capacity of plants in the C3 and  
160 C4 photosynthetic pathways to convert incident light energy and other resources  
161 into biomass (Ogutu et al., 2013). The use of  $FAPAR_{ps}$  accounts for APAR that is  
162 absorbed by photosynthesising parts of the vegetation canopy while a quantum  
163 yield term in this case reduces uncertainties due to land cover misclassification  
164 since plants are treated only based on their photosynthetic pathways. In its basic  
165 form, the GPP from the model ( $GPP_{SCARF}$  g C m<sup>-2</sup> day<sup>-1</sup>), can be estimated following  
166 Ogutu et al. (2013):

$$167 \quad GPP_{SCARF} = PAR * FAPAR_{ps} * (a * k) \quad (1)$$

168 Where PAR ( $\mu\text{mol m}^{-2} \text{s}^{-1}$ ) is the incoming photosynthetically active radiation,  
169  $FAPAR_{ps}$  ( $\mu\text{mol m}^{-2} \text{s}^{-1}$ ) is time averaged absorbed active radiation (APAR) derived  
170 as a product of fraction of APAR absorbed only by photosynthesising tissue in the

171 canopy,  $a$  ( $\mu\text{mol } \mu\text{mol}^{-1}$ ) is the maximum quantum yield for either C3 or C4 plants  
172 and  $k$  represents modifying conditions affecting maximum quantum yield.  
173 Parameters  $a$  and  $k$  in above equation can be expanded to:

$$174 \quad a = P_{C3} a_{C3} f_{C3}^{vpd} \Psi_e \quad (2)$$

$$175 \quad k = (1 - P_{C3}) a_{C4} f_{C4}^{vpd} \quad (3)$$

176 Where  $P_{C3}$  represents the proportion (%) of C3 plants,  $(1-P_{C3})$  represents the  
177 proportion of C4 plants within a study site,  $a_{C3}$  and  $a_{C4}$  represent the maximum  
178 quantum yields for C3 and C4 plants, respectively,  $\Psi_e$  (unitless) is the influence of  
179 temperature and leaf  $\text{CO}_2$  concentration on the maximum quantum yield of C3  
180 plants.  $f_{C3}^{vpd}$  and  $f_{C4}^{vpd}$  represent the influence of vapour pressure deficit (VPD) on  
181 C3 and C4 photosynthesis, respectively.

182 C3 and C4 plants are essentially separated by their distinct photosynthetic  
183 responses to temperature and  $\text{CO}_2$  partial pressure at the leaf surface.  $\text{CO}_2$  partial  
184 pressure in the chloroplast is 5-10 times higher in C4 than in C3 photosynthesis  
185 and this efficiently prevents photorespiration due to suppression of oxygen  
186 competition and saturation of Rubisco carboxylase activity (Ehleringer & Björkman,  
187 1977). Since the process of photorespiration is both temperature and  $\text{CO}_2$   
188 dependent, photosynthesis is generally higher in C4 than C3 plants at high  
189 temperature and low  $\text{CO}_2$  partial pressure (Brooks & Farquhar, 1985). The values  
190 adopted in the SCARF Model to parameterise  $a_{C3}$  and  $a_{C4}$  ( $0.08 \text{ mol mol}^{-1}$  and  
191  $0.06 \text{ mol mol}^{-1}$  respectively) concur with both laboratory and field based  
192 measurements (Collatz et al., 1991; Collatz et al., 1992; Ehleringer & Björkman,  
193 1977).



194

195 *2.1.1. Sub-models*

196 A number of sub-models were incorporated in the SCARF Model and these included  
197 Vapour Pressure Deficit (VPD),  $FAPAR_{ps}$  and  $\psi_e$  which estimate the influence of  
198 temperature and leaf CO<sub>2</sub> concentration on the maximum quantum yield of C3  
199 plants.

200 *2.1.1.1. The Vapour pressure deficit sub model*

201 Vapour Pressure Deficit (VPD) is a key physiological variable used in ecosystem  
202 productivity models as it is directly related to environmental stress. It can be  
203 defined as the difference (deficit) between the amount of moisture in the air and  
204 how much moisture the air can hold when it is saturated. It brings together the  
205 effects caused by both relative humidity and temperature as a single indicator of  
206 plant health. High VPD causes plant leaves to reduce stomatal aperture to regulate  
207 excessive water losses through transpiration (T) which in turn reduce CO<sub>2</sub>  
208 assimilation for photosynthesis. To incorporate the effect of VPD on the quantum  
209 yield, a sigmoid function was adopted since high VPD causes moisture stress in  
210 the plant, and therefore inhibits photosynthesis, while low VPD will generally result  
211 in an increase in photosynthesis but tends to flatten out with continued decrease.  
212 In the original SCARF model the VPD function was parameterised using the  
213 equation below (Ogutu et al., 2013; Tu, 2000):

214

$$f_v(Dk) = \frac{1}{1 + \exp[1.3(VPD_{213})]} \quad (4)$$

216 Where  $VPD$  (Pa) is the instantaneous moisture condition

217 For site level evaluation of the model, in-situ VPD observations were used.  
218 However, for application at the regional scale, VPD values used were estimated  
219 following Unwin (1980) whereby VPD is expressed as the difference between  
220 saturation vapour pressure (SVP) and actual vapour pressure (AVP). SVP (Pa) is  
221 calculated as follows:

$$222 \quad SVP = 6.11 * \exp((L./Rv) * (1./273 - 1/(273.15 + T))) \quad (5)$$

223 Where L is latent heat of vaporisation ( $2.5 * 10^6 \text{ Jkg}^{-1}$ ), Rv is a gas constant for  
224 water vapour ( $461 \text{ JK}^{-1} \text{ kg}^{-1}$ ) and T is air temperature ( $^{\circ}\text{C}$ ). AVP (Pa) is calculated  
225 as:

$$226 \quad AVP = (RH/100) * SVP \quad (6)$$

227 Where RH is relative humidity (%), calculated as follows:

$$228 \quad RH = 100 * (\exp((17.625 * DPT)/(243.04 + DPT)) / \exp((17.625 * T)/(243.04 + T))) \quad (7)$$

229 Where DPT is dew point temperature ( $^{\circ}\text{C}$ )

230 Evaluation of estimated VPD against those derived from the measurements at the  
231 flux tower was performed for seven sites and the agreement was considered as  
232 modest to very good ( $R^2=0.61$  to  $0.96$ ).

#### 233 *2.1.1.2. FAPAR<sub>ps</sub> sub-model*

234 FAPAR<sub>ps</sub> for a canopy has a strong linear relationship with the total quantities of  
235 chlorophyll present in that canopy (Ogutu et al., 2013). The MTCI has been used  
236 as a surrogate for GPP and chlorophyll content (e.g. Dash et al., 2010; Harris &  
237 Dash, 2010, 2011) and FAPAR<sub>ps</sub> (e.g. Ogutu et al., 2013) yielding strong positive  
238 relationship. The current study assumes MTCI to be a proxy for FAPAR<sub>ps</sub>. A full  
239 description of how FAPAR<sub>ps</sub> was derived through the inversion of EC NEE data and

240 related to MTCI can be found in Ogutu et al. (2013). The relationship between  
241 FAPAR<sub>ps</sub> and MTCI derived in Ogutu et al (2013) as shown below was used in the  
242 current study.

$$243 \quad fAPAR_{ps} = 0.76 * MTCI + 0.07 \quad (8)$$

#### 244 *Influence of temperature on C3 photosynthesis*

245 To estimate the influence of temperature and CO<sub>2</sub> partial pressure on the  
246 maximum quantum yield of C3 photosynthesis, the term  $\psi_e$  was incorporated  
247 following (Hanan et al., 1998)

$$248 \quad \psi_e = -0.0043049 T - 0.0002077 T^2 + 0.8973228 \quad (9)$$

249 Where  $T$  is the atmospheric air temperature. The model was implemented at the  
250 site level by using *in-situ* temperature measurements, while at continent scale by  
251 using European Centre for Medium-Range Weather Forecasts (ECMWF) reanalysed  
252 air temperature measured at 2m above the ground surface.

#### 253 **2.2. Eddy covariance flux data**

254 Seven EC flux sites (with data covering a total of 15 years) within the  
255 CARBOAFRICA flux network were used in the analyses (Table 1). These sites  
256 measure fluxes in some of the dominant and typical representative ecosystems  
257 across Africa. The study was primarily depended upon coincident data available  
258 for flux data and the MERIS MTCI data which is a dominant variable from which  
259 GPP is computed. The Tchizalamou (CG-Tch) in the Republic of Congo represents  
260 tropical grassland ecosystems in central-west Africa while the Bontioli site in  
261 Burkina Faso (BF-Bon) and Demokeya in Sudan (SD-Dem) take measurements in  
262 sub-humid and semi-arid Sahel climates, respectively. Mongu in Zambia (ZM-Mon),

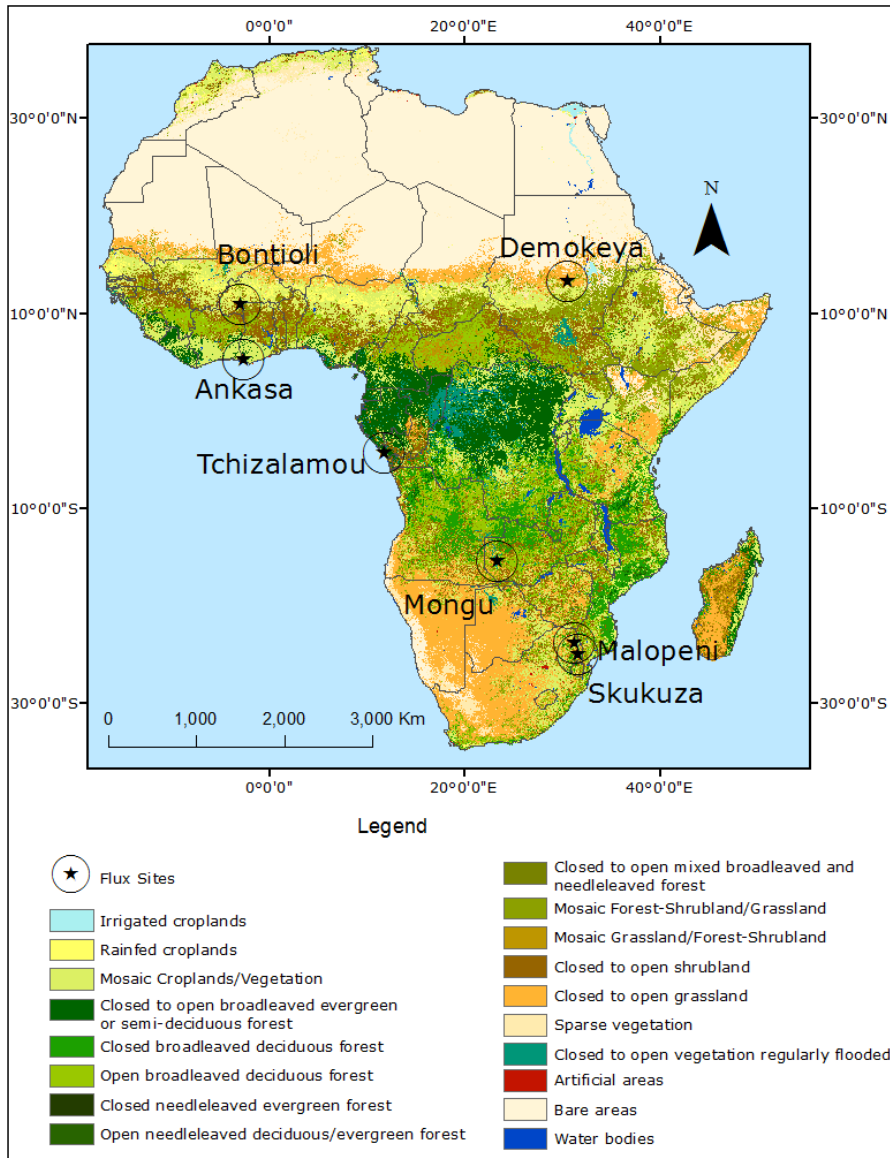
263 Malopeni (ZA-Map) and Skukuza (ZA-Kru), both in South Africa, represent sub-  
264 humid and semi-arid savannas of southern Africa while Ankasa site in Ghana (GH-  
265 Ank) represents tropical rain forest ecosystems. Due to the scarcity of flux tower  
266 sites in Africa, no data was available for the tropical dryland forests in Africa.  
267 Therefore, the model was not calibrated and validated for this biome and due to  
268 this, the SCARF model results for this biome may contain uncertainties.

269 The selected EC data are gap-filled CARBOAFRICA Level 4 datasets which are  
270 available at different temporal scales including 30 minutes, daily, weekly as well  
271 as monthly scales. GPP is calculated from NEE values computed either using the  
272 one-point or profile approach in the storage term computation (standardized and  
273 original NEE respectively) (Papale et al., 2006). Gap filling of the NEE  
274 measurements is then achieved through Marginal Distribution Sampling (MDS)  
275 and Artificial Neural Network (ANN). This study used GPP values estimated from  
276 standardized NEE and then gap-filled using the MDS method. A detailed  
277 description of the level 4 CARBOAFRICA dataset and its original processing is given  
278 in Papale et al. (2006).

279 Daily estimates of flux GPP were chosen for this study and values were then  
280 aggregated by calculating the mean value to 10-day (dekadal) time steps to  
281 coincide with the MERIS MTCI data. Flux GPP values were also aggregated by  
282 calculating the mean to 8-day time steps to match MOD17 GPP product since it  
283 was also used to evaluate the performance of the SCARF model. However, for PAR  
284 values, level 2 dataset was used (i.e. the 30 minute averages of photosynthetic  
285 photon flux density (PPFD,  $\mu\text{mol m}^{-2} \text{s}^{-1}$ ) after being aggregated to daily and  
286 decadal averages. Table 1 gives the main characteristics while Figure 1 shows the  
287 distribution and locations of the participating sites.

289 **Table 1:** Main characteristics of the seven evaluation flux tower sites

Site	Country	Lat	Lon	Ecosystem	C3/C4 cover	MAP (mm)	MAT (°C)	Years	References
Tchizalamou	Dem Rep Of Congo	-4.2892	11.6564	Tropical-humid grassland	0/100	1150	26	2006-2010	(Merbold et al., 2009)
Bontioli	Burkina Faso	10.1822	-3.6727	Sub-humid Savanna	70/30	926	26.1	2008	(Brummer et al., 2008; Papale et al., 2006)
Demokeya	Sudan	13.2829	30.4783	Semi-arid savanna	30/70	320	26	2005-2008	(Ardö et al., 2008)
Skukuza	South Africa	-25.0197	31.4969	Sub-humid wooded savanna	30/70	545	22	2006-2008	(Papale et al., 2006)
Malopeni	South Africa	-23.8325	31.2145	Sub-humid savanna	30/70	458	22.2	2009	(Papale et al., 2006)
Mongu	Zambia	-15.4377	23.2527	Sub-humid woodland	95/5	945	24.5	2006-2008	(Papale et al., 2006)
Ankasa	Ghana	5.2697	-2.6948	Tropical evergreen forest	100/0	1900	26	2011	(Chiti et al., 2010; Fattore et al., 2014)



291

292 **Figure 1:** A GlobCover map of Africa showing generalised land cover types and

293 the locations of flux tower sites used in evaluation exercise

294

295

### 296 **2.3. Meteorological data**

297 A number of meteorological measurements including daily mean of atmospheric  
298 temperature ( $T_a$ , °C), PAR ( $\mu\text{mol m}^{-2} \text{s}^{-1}$ ), VPD (hPa) and dew point temperature  
299 (DPT, °C) were used for this study. *In-situ* measurements of  $T_a$ , VPD and PAR  
300 recorded at the flux site were direct input variables in the SCARF model for site  
301 level evaluation. However, for modelling GPP across coterminous Africa,  $T_a$  and  
302 VPD were obtained from ECMWF website ([http://data-  
303 portal.ecmwf.int/data/d/interim\\_full\\_daily/](http://data-portal.ecmwf.int/data/d/interim_full_daily/)) at full resolution ( $0.75^\circ \times 0.75^\circ$  grids).  
304 DPT data was used in a sub-model to estimate VPD since there was no readily  
305 available product for VPD. A GLASS PAR product (Liang & Zhang, 2012), which is  
306 freely available at <ftp://ftp.glcfc.umd.edu/glcfc/GLASS/PAR/>, with a 5km spatial and  
307 3 hours temporal resolution was also used to control rate of photosynthetic  
308 conversion in the model at continent scale. Daily images acquired at 12 noon and  
309 aggregated to monthly averages were used. Pixels with zero/missing values were  
310 omitted in the statistics. Further details about the GLASS PAR product can be  
311 found in (Liang & Zhang, 2012; Liang et al., 2006).

312 All raster grids were resampled to match the 1km x 1km ground resolution of the  
313 MTCI data.

### 314 **2.4. Land cover data and determination of C3/C4 proportions**

315 Land cover information was derived from a 2009 GlobCover map obtained from  
316 the European Space Agency (ESA) GlobCover Portal Website  
317 (<http://due.esrin.esa.int/globcover/>). The data has a ground pixel size of 300m  
318 and was used for two purposes. Firstly, to derive maps of C3 and C4 distribution

319 and their relative proportions in each 1km grid cell, and secondly to define pixel-  
320 based maximum quantum yields for C3 and C4 photosynthesis. The C3/C4  
321 proportions used for site level implementation of the model (Table 1) were based  
322 on figures published in Merbold et al. (2009). To estimate the relative proportions  
323 of C3/C4 plants in each 1km<sup>2</sup> pixel, first the land cover map was reclassified into  
324 C3, C4 and C3/C4 maps. The C3 map contained all pixels dominated by forests  
325 and woodlands, while the C4 map contained all pixels dominated by grasslands.  
326 The C3/C4 map contained all pixels with mixed savannas and all cropland. Since  
327 the land cover map does not specify vegetation composition in areas where  
328 mosaics of grasslands, shrublands and forests, a 50-50 ratio between C3/C4 was  
329 assumed in these pixels. The same assumption was also made for cropland  
330 because both C3 and C4 crops are widely grown across Africa but their distribution  
331 is not specified in the land cover map.

## 332 **2.5. Data Processing**

### 333 ***2.5.1. Processing of MTCI time series data***

334 The 1km dekadal original MTCI data were provided by the Natural Environmental  
335 Research Council Earth Observation Data Centre (NERC NEODC) - [ftp://13-  
336 server.infoterra.co.uk/pub/](ftp://13-server.infoterra.co.uk/pub/)) of the European Space agency (ESA) and processed  
337 by Astrium GEO-Information Service. The MTCI Level 2 product was calculated  
338 using three red/near infra-red bands of the ENVISAT MERIS data to produce an  
339 image indicating the amount of chlorophyll content per unit area (Curran & Dash,  
340 2005).

341 A considerable amount of error is usually expected in any efforts of up-scaling  
342 point measurements obtained from a flux tower to the spatial scale of the satellite  
343 pixel e.g. the 1km x 1km extent of the MTCI images. Since it is difficult to identify



344 the exact pixel from which the flux tower measurements are made, a 3x3 km  
345 sample, whose centre is at the respective tower location, was extracted and  
346 averaged (zero values were excluded) to get a representative value to correspond  
347 with the tower GPP. Visual inspection of each flux site on Google Earth also  
348 confirmed that all the sites were homogeneous for at least 1km in any direction  
349 from each respective site. A separate assessment based on 2005 MODIS land  
350 cover product also confirmed that at least 88% of the pixels in the 3x3km grid  
351 had the same land cover value as the centre (flux tower) pixel.

### 352 ***2.5.2. Processing MODIS GPP time series data***

353 The MOD17 GPP Version 6 Product was obtained from both the NASA Earthdata  
354 Search portal (<https://search.earthdata.nasa.gov/search?q=MOD17A2H+V006>)  
355 and Oak Ridge National Laboratory Distributed Active Archive Centre's (ORNL  
356 DAAC, MODIS Land Subsets ([https://modis.ornl.gov/cgi-  
357 bin/MODIS/global/subset.pl](https://modis.ornl.gov/cgi-bin/MODIS/global/subset.pl))). The Version 6 product is at 500m resolution,  
358 therefore a 1.5 x 1.5 km sample, centred at each respective flux site, was used to  
359 extract time series GPP values for these sites. The MOD17 GPP values were  
360 available in kg C m<sup>-2</sup> in 8 days and were converted to g C m<sup>-2</sup> day<sup>-1</sup> to be consistent  
361 with the GPP measured by the EC technique.

### 362 ***2.5.3. Sensitivity and uncertainty analyses***

363 The overall importance of an input parameter in a model can be assessed based  
364 on its impact on the model output. One way of achieving this is to test how much  
365 of the model output is explained by a parameter through regression analysis of  
366 the input parameter with the model output. The other method is to allow one  
367 parameter to vary at a time while others are held constant (e.g. Hamby, 1993).  
368 In this study, the regression method was employed. Modelled GPP values were

369 regressed against  $T_a$ , PAR, VPD and MTCI and the statistics on goodness of fit were  
370 determined.

371 The Monte Carlo technique was also used to assess the degree of sensitivity and  
372 uncertainty of GPP due to the quantum yield parameters for C3 and C4 plants ( $a_3$   
373 and  $a_4$ , respectively) at all seven study sites. The maximum quantum yields ( $a_3$   
374 =0.08 and  $a_4$  =0.06 $\mu\text{mol } \mu\text{mol}^{-1}$ ) used in the initial evaluation of the SCARF model  
375 (Ogutu et al., 2013) are based on laboratory and field experiments carried out for  
376 different vegetation types from different ecosystems, mostly outside the African  
377 environments. The main concern for the current work is related to the stochasticity  
378 associated with these parameters since they are not fixed but may vary with time  
379 and space. Given the diversity and heterogeneity of the ecosystems considered in  
380 this study, an attempt was made to estimate the biases associated with the  
381 inaccuracies and unavoidable random variation in the use of the two maximum  
382 quantum yields.

383 According to published literature, values of  $a_3$  vary from a minimum of 0.0525 to  
384 a maximum of 0.08 while  $a_4$  varies from 0.0535 to 0.065 (Ehleringer & Björkman,  
385 1977; Ehleringer & Pearcy, 1983;Singsaas et al., 2001). To determine the  
386 variability in output that result from the two parameters, 500 random samples  
387 were generated for each parameter based on ranges of the documented values  
388 and 500 model runs were performed based on the randomly generated samples.  
389 Mean, standard deviation, root mean square error (RMSE) and range were  
390 computed for the modelled GPP and compared to *in-situ* GPP for each site. The  
391 'best guess' for each random parameter and site was determined based on the  
392 model run with the smallest RMSE calculated between observed and modelled GPP

393 for each participating flux site. The implementation of the model at both site and  
394 regional scale was thus based on the 'best guesses' of  $a_3$  and  $a_4$  for different  
395 ecosystems.

396

### 397 **3. Results**

#### 398 **3.1. Model sensitivity and uncertainty analyses**

##### 399 *3.1.1. Importance of different parameters to model output*

400 The sensitivity of  $GPP_{SCARF}$  to the main environmental drivers changes substantially  
401 through time and among ecosystems. A fundamental distinction can be noted  
402 between moisture stressed and water sufficient ecosystems particularly in relation  
403 to their response to VPD, PAR and  $T_a$ . VPD has weak to very strong negative  
404 relationships ( $-0.17 > R^2 > -0.99$ ) against  $GPP_{SCARF}$  in sub-humid and semi-arid  
405 ecosystems (i.e. Mongu, Demokeya, Skukuza, Bontioli, and Malopeni) while it  
406 exhibits modest positive correlations in tropical humid grassland (Tchizalamou)  
407 and rain forest (Ankasa) ecosystems ( $R^2=0.61$  and  $0.40$ , respectively) (Table 2).  
408 The difference between the responses of these ecosystems can be explained by  
409 how the vegetation attempts to optimise  $CO_2$  uptake and water loss in response  
410 to changing moisture conditions. In water sufficient areas, increasing VPD would  
411 increase stomatal conductance ( $g_s$ ) (and ET) but since plants do not initiate  
412 stomatal resistance owing to sufficient soil moisture, rate of  $CO_2$  assimilation  
413 increases. VPD is particularly important in the sub-humid and semi-arid savanna  
414 ecosystems of Bontioli and Demokeya ( $R^2=-0.99$  and  $-0.94$ , respectively) (Table  
415 2) where  $T_a$  and PAR are constantly high throughout the year.

416 The response of  $GPP_{SCARF}$  to  $T_a$  almost always mirror that of PAR even though the  
417 correlation coefficients differ in absolute values. Both PAR and temperature have  
418 strongest positive correlation in tropical humid and rainforest ecosystems (i.e.  
419 Chizalamou and Ankasa - Table 2). These two sites have a relatively wet and  
420 cloudy climate compared to the other study sites. These conditions result in  
421 increased relative humidity, cloudiness and precipitation incidences which in turn  
422 reduce temperature and available PAR. Therefore, temperature and PAR are  
423 important in determining the levels of primary productivity in these sites. As  
424 expected, both  $T_a$  and PAR had a negative correlation with  $GPP_{SCARF}$  in the sub-  
425 humid and semi-arid ecosystems (i.e. Mongu, Demokeya, Skukuza, Bontioli, and  
426 Malopeni) as high PAR and  $T_a$  may cause photoinhibition and high ET/VPD,  
427 respectively in these water limited ecosystems.

428 The model's sensitivity to MTCI is highest in savanna woodland ecosystems,  
429 moderate in tropical grassland and weak in tropical rain forests. However, of  
430 importance is the fact that while response of GPP to MTCI is both strong and  
431 positive in all other ecosystems, it is negative in tropical rainforests (Table 2). As  
432 the vegetation in tropical evergreen forests has high chlorophyll concentration and  
433 multi-layered canopies, most of the incident light energy is absorbed by  
434 chloroplasts at the top of the canopy while deep layers are deprived of light energy.  
435 This may suggest that photosynthesis could be quite high at the top most layers  
436 of the canopy but overall productivity is reduced due to decreased photosynthetic  
437 rates within the deep and under storey owing to light deprivation.

438

439

440

441 **Table 2.** Importance of the various input parameters as determined by the  
 442 coefficient of determination ( $R^2$  values) between time series of  $GPP_{SCARF}$  and main  
 443 meteorological and vegetation biophysical parameters

Flux Site	n (10-day time step)	Coefficient of determination ( $R^2$ values) between $GPP_{SCARF}$ and			
		PAR	VPD	MTCI	Temperature
Mongu	68	-0.18	-0.77	0.89	-0.22
Tchizalamou	85	0.91	0.61	0.65	0.86
Demokeya	78	-0.07	-0.94	0.75	-0.03
Skukuza	59	-0.65	-0.22	0.92	-0.59
Bontioli	22	-0.42	-0.99	0.94	-0.52
Malopeni	31	-0.60	-0.17	0.57	-0.51
Ankasa	33	0.86	0.40	-0.25	0.61

444

445

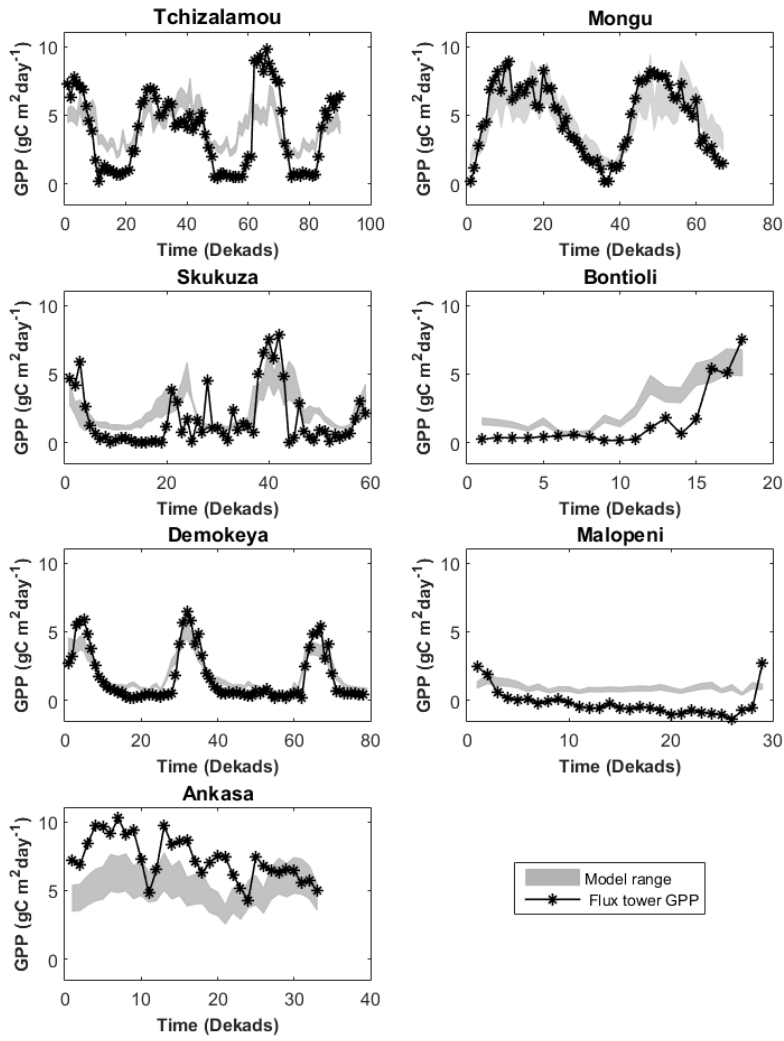
446 *3.1.2. Uncertainties resulting from the quantum yield terms*

447 The model variability due to the uncertain quantum yield terms was achieved  
 448 based on 500 random samples generated between acceptable ranges for  $a_3$  and  
 449  $a_4$  from which 500 model runs were subsequently performed for each site (Figure  
 450 2). The importance of the two parameters was both site and season dependent.  
 451 For example, both parameters were more important at Mongu, Bontioli,  
 452 Tchizalamou and Demokeya during the main growing season when the estimated

453 GPP was within one standard deviation of the modelled GPP (Figure 2). During the  
454 senescence stages, observed GPP was outside the model range indicating that, as  
455 expected, maximum quantum yields of both C3 and C4 were no longer main  
456 determinants of GPP. Other parameters closely linked to seasonality especially  
457 FAPAR<sub>ps</sub> (chlorophyll content) and VPD make it impossible to achieve maximum  
458 photosynthetic rates during the senescence stages of plant development. VPD was  
459 identified as the main cause of overestimation of GPP during the dry season in  
460 European and North American ecosystems during the initial evaluation of the  
461 SCARF model (Ogutu et al., 2013). The same trend is observed for ecosystems  
462 represented in the current study. The only difference, though, is that the model  
463 range is larger especially in ecosystems dominated by C3 species. This could be  
464 expected given the range of uncertainty for  $a_3$  (0.053 to 0.08 mol mol<sup>-1</sup>)  
465 compared to  $a_4$  (0.053 to 0.065 mol mol<sup>-1</sup>).

466 'Best guesses' of maximum quantum yields for C3 and C4 photosynthesis, as  
467 represented by model runs with smallest RMSE, indicate a consistent  $a_3$  of 0.0543  
468 and  $a_4$  of 0.0532 across all mixed savanna sites while an  $a_3$  of 0.08 and  $a_4$  of  
469 0.056 were observed for the woodland sites of Mongu and Bontioli. Tropical sites  
470 of Tchizalamou and Ankasa with 100% proportions of C3 and C4 plants,  
471 respectively, returned near-maximum values for both  $a_3$  and  $a_4$  owing to little  
472 influence resulting from heterogeneity in vegetation composition and structure as  
473 in the savannas.

474



475

476 **Figure 2.** Simulated and observed GPP for flux tower sites. The grey area marks  
 477 the range of GPP from two hundred model runs.

478

479

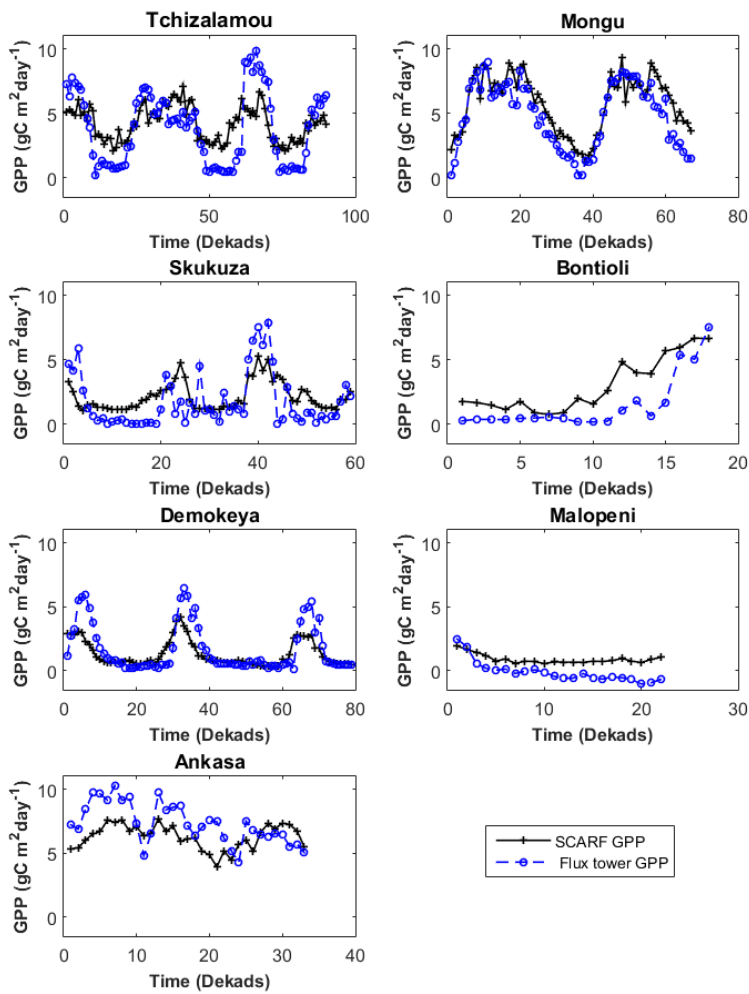
480 **3.2. Seasonal and annual variability of model GPP across Africa**

481 SCARF model GPP was evaluated against *in-situ* flux measurements at seven flux  
482 sites. Overall, GPP<sub>SCARF</sub> values show good agreement with observed GPP at most  
483 sites (except tropical rainforest site) in terms of seasonality (Figure 3) and  
484 absolute values (Figure 4). There is good coincidence between predicted GPP  
485 peaks and growth season as well as troughs within low growth seasons (Figure 3).  
486 Mean daily GPP across the investigated period varied significantly across sites from  
487 a minimum of 0.44 gC m<sup>-2</sup> day<sup>-1</sup> at the semi-arid and sub-humid savanna  
488 grassland sites to a maximum of 9.86 gC m<sup>-2</sup> day<sup>-1</sup> at the woodland and tropical  
489 rain forest sites. The highest seasonal at-site variability was observed at  
490 Tchizalamou and least variability was observed at Malopeni (Figure 3).

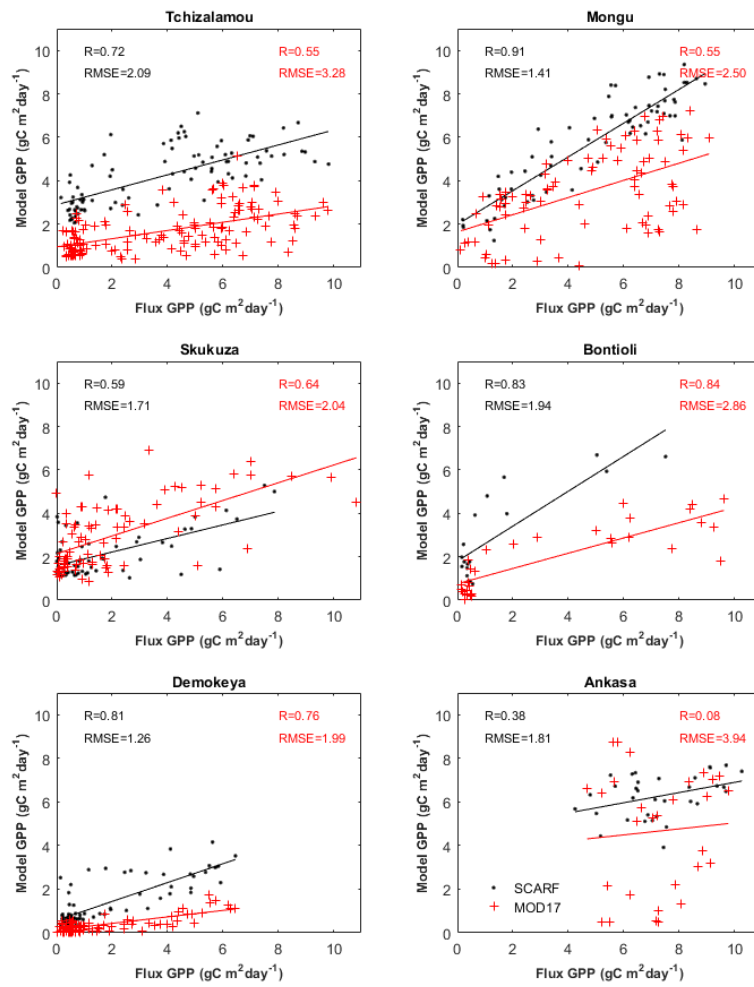
491 The SCARF model output have modest to very strong positive correlation with  
492 observed GPP at most sites (R 0.59 to 0.91, p <0.0001) apart from the tropical  
493 rainforest site (R = 0.38, p=0.02). The comparison between MOD17 product and  
494 *in-situ* flux tower GPP estimates resulted in slightly lower R<sup>2</sup> and higher RMSE  
495 values in most of the sites (Figure 4). Overall, the MOD17 product tended to  
496 underestimate GPP in most of the evaluated sites (Figure 4). For the SCARF model,  
497 the coefficient of correlation between the model data and the flux tower estimates  
498 were strongest (R>0.83, p<0.0001) in savanna biomes dominated by woody  
499 species (i.e. Mongu and Bontioli), moderate (R> 0.5, p<0.0001) in more  
500 heterogeneous grassland and savanna ecosystems (i.e. Skukuza, Demokeya, and  
501 Tchizalamou) and low (R = 0.38, p = 0.02) in the evergreen rainforest site (i.e.  
502 Ankasa) (Figure 4). For the MOD17 product strong correlation (R> 0.76, p<0.0001)  
503 was observed in the savanna site of Demokaya and wooded savanna site of  
504 Bontioli, moderate correlation (R> 0.55, p<0.0001) at Tchizalamou, Mongu and



505 Skukuza and weak correlation ( $R = 0.08$ ,  $p = 0.698$ ) at the evergreen tropical  
 506 forest site (i.e. Ankasa) (Figure 4). Overall, the correlation coefficients were  
 507 strongest in ecosystems where vegetation follows a prescribed seasonal cycle as  
 508 determined by canopy chlorophyll content and leaf area index.



509  
 510 **Figure 3:** Seasonal and spatial trends of *in-situ* and SCARF model GPP for flux  
 511 tower sites.

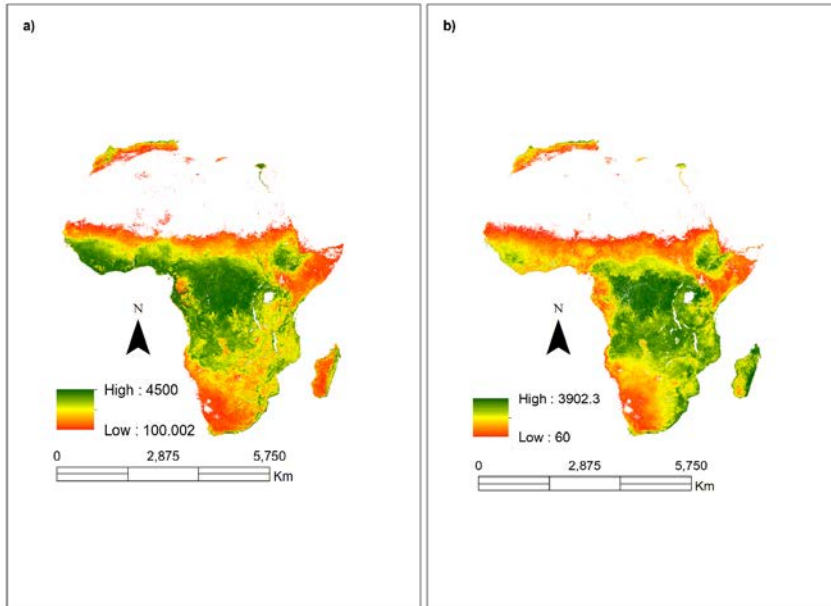


514 **Figure 4:** Relationship between SCARF model output (black dots), MOD17 (red  
 515 asterisks) and *in-situ* flux tower GPP measurements at various sites.

517

518 **3.3. Spatial distribution of GPP across Africa**

519 Figure 5 (*a* and *b*) show the distribution of GPP predicted by the SCARF model and  
520 MOD17 product, respectively. The distribution of  $GPP_{SCARF}$  across the coterminous  
521 Africa concur with the findings from the site level analysis where highest GPP  
522 values are concentrated in the central tropical rain forests, moderate values within  
523 pixels dominated by woody species and lower productivity in grasslands and  
524 sparsely vegetated areas. SCARF model has higher absolute values in most of the  
525 sub-humid and semi-arid savanna ecosystems and parts of the tropical rain forests  
526 while MOD17 GPP depicts higher values in isolated regions for example on the  
527 island of Madagascar. Overall,  $GPP_{SCARF}$  has a minimum GPP of  $100 \text{ g C m}^{-2} \text{ yr}^{-1}$  and  
528 maximum of  $4,500 \text{ g C m}^{-2} \text{ yr}^{-1}$  compared to 60 and  $3,900 \text{ g C m}^{-2} \text{ yr}^{-1}$  from the  
529 MOD17 product. The total annual GPP predicted by the SCARF model for the year  
530 2010 was  $35.25 \text{ Pg C yr}^{-1}$  and that from MOD17 was  $21.39 \text{ Pg C yr}^{-1}$ , showing that  
531 SCARF model prediction was higher than that from MOD17 product.



532

533 **Figure 5:** Spatial distribution of annual sum GPP ( $\text{g C m}^{-2} \text{yr}^{-1}$ ) from (a) SCARF  
 534 model and (b) MOD17 product for period January to December 2010

535

536

537 **4. Discussion**

538 **4.1. Model sensitivity and uncertainty**

539 Analyses of the importance of different biophysical and meteorological input  
 540 parameters on  $\text{GPP}_{\text{SCARF}}$  show that VPD has negative influence at most of the sub-  
 541 humid and semi-arid ecosystems ( $R^2 = -0.17$  to  $-0.99$ ) which is consistent with  
 542 other studies, for example, Sjöström et al. (2013). The relationship was expected  
 543 since moisture availability is the main controller of vegetation seasonality and

544 development in these ecosystems (e.g. Ibrahim et al., 2015; Merbold et al., 2009;  
545 Scholes et al., 2004). A negative relationship between GPP and  $T_a$ , was observed  
546 in the semi- arid and sub-humid ecosystems. Similar relationships were also  
547 observed between GPP and PAR at these sites. In these ecosystems, high  
548 temperature coupled with low moisture availability will act to reduce GPP. However,  
549 there was a positive relationship between  $T_a$  and GPP at two sites (i.e. Ankasa and  
550 Tchizalamou). In these sites, the wet and cloudy climate tends to reduce  
551 temperature and PAR, hence the observed positive relationship between GPP and  
552 the two variables.

553 The model output had modest to very strong positive correlations with MTCI  
554 ( $R^2=0.57$  to  $0.94$ , MTCI is used as a  $FAPAR_{ps}$  surrogate in the model). A weak  
555 negative relationship ( $R^2=-0.25$ ) between MTCI and model GPP observed at a  
556 tropical rainforest site (Ankasa) suggests that chlorophyll content ceases to be the  
557 dominant determinant of GPP in this biome. The initial validation of the SCARF  
558 Model (Ogutu et al., 2013) also documented weaker correlations ( $R^2=0.60$ ) of  
559 model results with flux measurements for evergreen needle leaf forests. Given the  
560 minimal fluctuations of chlorophyll content in evergreen forests, the model may  
561 predict high GPP even during periods of low productivity resulting in poor  
562 correlations. This theory may explain the increase in model  $GPP_{SCARF}$  around dekad  
563 25 to 33 at Ankasa (Figure 3) while observed GPP shows a gradual decline.

564 A stronger correlation of PAR with  $GPP_{SCARF}$  at the evergreen ecosystem ( $R^2=0.86$ )  
565 may suggest that while MTCI may cease to be the most important parameter in  
566 tropical rainforest productivity, light availability plays a more important role.  
567 Tropical rainforest ecosystems show indications that light could be a major limiting  
568 factor to photosynthesis during the wet season. Reduced incident light energy at

569 the canopy may result due to both high incidences of cloudiness and/or high  
570 chlorophyll concentrations that will deprive light to understorey vegetation. Light  
571 available to individual leaves in a canopy decreases according to the Beer's law of  
572 light extinction and given the high leaf area index reported in tropical rain forests  
573 (e.g. LAI >6; Clark et al., 2008), the under storey may be completely deprived of  
574 light energy. While high chlorophyll content may increase photosynthesis at the  
575 top most canopy layers, total productivity may decline as a result of very low  
576 photosynthetic activity in the deeply buried understorey ( DeLucia and Thomas,  
577 2000; Kim et al., 2016). The high GPP values occurring from decade 5 to 15  
578 coincide with the low rainfall season at Ankasa. This suggests that the vegetation  
579 canopy intercepts more radiation owing to reduced cloud condition resulting in  
580 increased vegetative growth.

581 The initial evaluation of the SCARF model undertaken by Ogutu et al., (2013)  
582 assumed a uniform distribution of the maximum quantum yields for C3 and C4  
583 without accounting for regions/pixels with considerable heterogeneity for example  
584 mixed savannas or croplands. In the current study, efforts to differentiate  
585 quantum yields for different ecosystems were made for two main reasons; first  
586 the maximum quantum yields can vary based on random occurrences of  
587 environmental and climatological factors (Collatz et al., 1991, 1992; Ehleringer &  
588 Bjorkman, 1977) and, second, African ecosystems depict huge variations and  
589 heterogeneity through space. The results showed that the influence of quantum  
590 yield on modelled GPP was both site and season dependent. The heterogeneous  
591 sites (i.e. mixed savanna and woodland sites) did not achieve their maximum  
592 quantum yield value during the model simulations. The homogenous sites (i.e. the  
593 tropical humid grassland and the evergreen forest sites) returned near-maximum

594 values for both  $a_3$  and  $a_4$ . Even though C4 photosynthesis is thought to reach  
595 maximum values in hotter environments like the ones investigated in this study,  
596 maximum  $a_4$  was not achieved at any of the savanna sites. This can be explained  
597 by the fact that savanna ecosystems depict considerable heterogeneity occurring  
598 over short spatial scales, sometimes in the order of a few metres (Desanker et al.,  
599 1997; Scholes et al., 2004; Walker, 1987). Under such conditions tree canopies  
600 often shade and control water and light availability for grasses and shrubs. Overall,  
601 the findings show the importance of varying the quantum yield value  
602 proportionally to the heterogeneity of the site when running the SCARF model.

603

#### 604 **4.2. Seasonal and inter-annual variability of model GPP across Africa**

605 An analysis of seasonal and inter-annual variability of  $GPP_{SCARF}$  shows that the  
606 model has capability to track seasonal changes in productivity across various  
607 biomes in Africa (Figure 3). Even though the dynamics of modelled GPP at each  
608 evaluated site depicted notable seasonal and ecosystem dependent trends, the  
609 model generally tended to overestimate dry season GPP across all seasonally dry  
610 ecosystems. This trend supports observations by Ogutu et al. (2013) over  
611 temperate regions. An explanation for this overestimation is that the use of VPD  
612 alone may not be adequate to control GPP in dry environments or during the dry  
613 season (Ogutu et al., 2013).

614 The comparison of absolute values of GPP predicted by the SCARF model and GPP  
615 estimated at flux tower sites showed a strong positive relationship ( $R > 0.59$ ,  
616  $p < 0.0001$ ) in all but one study site (i.e. Ankasa tropical forest,  $R = 0.38$ ,  $p = 0.02$ ).

617 The absolute GPP values predicted by the SCARF model ranged from  $0.44 \text{ gCm}^{-2}$

618 in low productivity sites (e.g. Malopeni svanna ecosystem) to  $9.86 \text{ gCm}^{-2}$  in high  
619 productivity sites (e.g. Ankasa rain forest). The correlation coefficients and error  
620 margins for the SCARF in the current study are also similar (or even better in other  
621 instances) as those reported in the initial evaluation of the model in North America  
622 and European ecosystems (Ogutu et al., 2013). However, the GPP absolute values  
623 predicted by the SCARF model for the northern latitudes (Ogutu et al., 2013) were  
624 considerably higher than those predicted by the SCARF model for African tropical  
625 regions in the present study. Similar trends have also been reported by Kicklighter  
626 et al.,(1999) and can be partially explained by the longer day length in the  
627 northern latitudes during summer. Evaluation of the SCARF model and the MOD17  
628 GPP product in their capability to represent GPP estimated at the studied flux tower  
629 sites showed that, in most cases, the output from the SCARF model was closer to  
630 the *in-situ* GPP (lower RMSE values) compared to the MOD 17 product (Figure 4).  
631 The MOD17 product tended to underestimate growing season GPP in most of the  
632 evaluated sites. Similar findings were reported in a comparison between SCARF  
633 model and MOD17 GPP model over Europe and USA (Ogutu et al., 2013). The  
634 main differences may be partly explained by the fact that the two models are  
635 premised on different assumptions regarding the interactions between input  
636 parameters as well as the sources of data used. For example, the MOD17 product  
637 uses  $f\text{APAR}_{ca}$  while  $\text{GPP}_{\text{SCARF}}$  is based on  $f\text{APAR}_{ps}$  and also the different techniques  
638 used to define the conversion of intercepted light (i.e. the LUE term).

639 Overall, the fact that the SCARF model shows a good capability to track the  
640 variability of GPP in the highly heterogeneous ecosystems in Africa, including the  
641 savannas which have been associated with high uncertainties in global estimates  
642 of carbon fluxes (Ciais et al., 2011; Merbold et al., 2009; Williams & Jackson,



643 2007), presents an opportunity to use the model improve GPP estimation across  
644 Africa.

645

#### 646 **4.3. Global and regional application of the SCARF Model**

647 The spatial variability of GPP predicted by the SCARF model in Africa (Figure 5)  
648 agrees with other maps from global models (e.g. Cramer et al., 1999; Huston &  
649 Wolverton, 2009) and the general pattern from the MOD17 model. The total  
650 annual GPP predicted by the SCARF model for Africa in 2010 was 35.25 Pg C yr<sup>-1</sup>,  
651 which was higher than annual GPP from MOD17 (21.39 Pg C yr<sup>-1</sup>). However, this  
652 values fall within those reported in previous studies. For example, a study by  
653 Valentini *et al* (2014) using a number of models reported that the mean annual  
654 GPP for Africa ranged from 20.61 to 40.91 Pg C yr<sup>-1</sup> with a mean of 28.16 Pg C yr<sup>-1</sup>  
655 for the year 1990-2009.

656 Even though the flux tower sites used in the current study were few, solid  
657 conclusions can be reached on the applicability of the SCARF model in African  
658 environments based on these sites as they represent the typical ecosystems of  
659 the continent. The scarcity of *in-situ* data available on African carbon fluxes  
660 remains a stumbling block in the quest to fully understand and improve GPP  
661 estimates for the continent. Therefore using models such as the SCARF model can  
662 help bridge this gap. The good performance of SCARF model in Europe and USA  
663 (Ogutu et al., 2013) and in Africa (this study) demonstrates its potential as a  
664 reliable diagnostic model that can be used to generate GPP estimates globally. The  
665 SCARF model has three advantages compared to existing PEMs. Firstly, it  
666 prescribes only two quantum yield terms (i.e. maximum quantum yield for C3 and  
667 C4 plants) to represent the rate of conversion of absorbed PAR into dry matter,

668 thereby eliminating the need for species specific LUE term. Secondly, it explicitly  
669 uses only the fraction of absorbed photosynthetic radiation absorbed by  
670 photosynthetic elements in the canopy (which is the actual PAR used in  
671 photosynthesis) as opposed to that of the total canopy. The use of FAPAR by  
672 photosynthetic elements in the canopy improves the accuracy of the model. Finally,  
673 the SCARF model does not require a detailed land cover map thereby limiting error  
674 propagation from inaccuracies in land cover classification. The recently launched  
675 SENTINEL satellites (i.e. SENTINEL 2 and 3) by the European Space Agency have  
676 spectral bands that can be used to derive key components of the SCARF model  
677 globally. This provides a unique opportunity to operationally produce global and  
678 regional GPP using the SCARF model at relatively high spatial resolution.

679

## 680 **5. Conclusion**

681 The study calibrated and applied the SCARF model to predict seasonal and spatial  
682 variability of GPP across African ecosystems. The SCARF model showed strong and  
683 positive correlation with *in situ* GPP measurements across most of the sites except  
684 at tropical rainforest ecosystem where a weak correlation was found. The seasonal  
685 variability of GPP was strongly connected to variability of main input parameters  
686 namely temperature, PAR, VPD and MTCI. The GPP from the model was negatively  
687 related to Temperature and PAR in water limited ecosystems. The influence of VPD  
688 on the SCARF model was varied across the ecosystem. Positive influence on GPP  
689 was observed in moisture sufficient ecosystems while negative influence in  
690 ecosystems that experience moisture deficit during part or most of the season.  
691 Monte Carlo analysis of the uncertainty in the model due to the choice of quantum  
692 yield parameters showed that these parameters varied more in heterogeneous

693 ecosystems compared to homogenous ecosystems. The SCARF Model shows great  
694 potential to improve GPP predictions across a wide range of natural ecosystems  
695 occurring in Africa as shown by a strong positive coefficient of correlation ( $R >$   
696  $0.59$ ,  $p < 0.0001$ ) in most ecosystems evaluated in this study. The annual GPP for  
697 Africa derived from the SCARF model (i.e.  $35.25 \text{ C yr}^{-1}$ ) was within the range of  
698 those reported in previous studies. This study has demonstrated the potential of  
699 an innovative approach to estimating carbon flux in understudied ecosystems of  
700 global importance. It comes at a timely moment, when relevant remotely sensed  
701 data (e.g. data from the Sentinel satellites by the European Space Agency) which  
702 can be used to parameterise such a model are becoming available and when the  
703 uncertainty associated with carbon flux measurement across the African continent  
704 is recognised as a major research challenge.

705

#### 706 **Acknowledgements**

707 The authors would like to thank the European Commission for providing  
708 scholarship, through the Erasmus Mundus Programme, which made it possible for  
709 P.C to undertake this research as part of his studies. Gratitude is also extended to  
710 the Principal Investigators (PIs) from the CARBOAFRICA flux network for providing  
711 flux datasets used for the evaluation exercise. The research was also made  
712 possible owing to data from different sources including ECMWF Reanalysis data,  
713 European Space Agency (ESA) GlobCover Portal, Natural Environmental Research  
714 Council Earth Observation Data Centre (NERC NEODC of the ESA, the Oak Ridge  
715 National Laboratory Distributed Active Archive Center's (ORNL DAAC) and GLASS  
716 PAR product.

717

718

719 **References**

- 720 Anav, A., Friedlingstein, P., Beer, C., Ciais, P., Harper, A., Jones, C., Murray-  
721 Tortarolo, G., Papale, D., Parazoo, N.C., Peylin, P., Piao, S., Sitch, S., Viovy, N.,  
722 Wiltshire, A., & Zhao, M. (2015). Spatiotemporal patterns of terrestrial gross  
723 primary production: A review. *Reviews of Geophysics*, 53, 785-818
- 724 Ardö, J., Mölder, M., El-Tahir, B.A., & Elkhidir, H.A.M. (2008). Seasonal variation  
725 of carbon fluxes in a sparse savanna in semi arid Sudan. *Carbon Balance and*  
726 *Management*, 3, 7
- 727 Asrar, G., Myneni, R.B., & Choudhury, B.J. (1992). Spatial heterogeneity in  
728 vegetation canopies and remote sensing of absorbed photosynthetically active  
729 radiation: A modeling study. *Remote Sensing of Environment*, 41, 85-103
- 730 Baldocchi, D., Reichstein, M., Papale, D., Koteen, L., Vargas, R., Agarwal, D., &  
731 Cook, R. (2012). The role of trace gas flux networks in the biogeosciences. *Eos,*  
732 *Transactions American Geophysical Union*, 93, 217-218
- 733 Baldocchi, D., Reichstein, M., Papale, D., Koteen, L., Vargas, R., Agarwal, D., &  
734 Cook, R. (2012). The role of trace gas flux networks in the biogeosciences. *Eos,*  
735 *Transactions American Geophysical Union*, 93, 217-218
- 736 Birch, E., & Wachter, S. (2011). World Urbanization: The Critical Issue of the  
737 Twenty-First Century. *Global Urbanization*, 3-23
- 738 Brooks, A., & Farquhar, G.D. (1985). Effect of temperature on the CO<sub>2</sub>/O<sub>2</sub>  
739 specificity of ribulose-1, 5-bisphosphate carboxylase/oxygenase and the rate of  
740 respiration in the light. *Planta*, 165, 397-406

741 Brümmer, C., Falk, U., Papen, H., Szarzynski, J., Wassmann, R., & Brüggemann,  
742 N. (2008). Diurnal, seasonal, and interannual variation in carbon dioxide and  
743 energy exchange in shrub savanna in Burkina Faso (West Africa). *Journal of*  
744 *Geophysical Research: Biogeosciences*, 113, n/a-n/a

745 Chiti, T., Certini, G., Grieco, E., & Valentini, R. (2010). The role of soil in storing  
746 carbon in tropical rainforests: the case of Ankasa Park, Ghana. *Plant and Soil*,  
747 331, 453-461

748 Ciais, P., Bombelli, A., Williams, M., Piao, S.L., Chave, J., Ryan, C.M., Henry, M.,  
749 Brender, P., & Valentini, R. (2011). The carbon balance of Africa: synthesis of  
750 recent research studies. *Philosophical Transactions of the Royal Society A:*  
751 *Mathematical, Physical and Engineering Sciences*, 369, 2038

752 Clark, D.B., Olivas, P.C., Oberbauer, S.F., Clark, D.A., & Ryan, M.G. (2008). First  
753 direct landscape-scale measurement of tropical rain forest Leaf Area Index, a  
754 key driver of global primary productivity. *Ecology Letters*, 11, 163-172

755 Collatz, G.J., Ball, J.T., Grivet, C., & Berry, J.A. (1991). Physiological and  
756 environmental regulation of stomatal conductance, photosynthesis and  
757 transpiration: a model that includes a laminar boundary layer. *Agricultural and*  
758 *Forest Meteorology*, 54, 107-136

759 Collatz, G.J., Ribas-Carbo, M., & Berry, J.A. (1992). Coupled Photosynthesis-  
760 Stomatal Conductance Model for Leaves of C<sub>4</sub> Plants. *Functional*  
761 *Plant Biology*, 19, 519-538

762 Coops, N.C., Ferster, C.J., Waring, R.H., & Nightingale, J. (2009). Comparison of  
763 three models for predicting gross primary production across and within forested

764 ecoregions in the contiguous United States. *Remote Sensing of Environment*,  
765 113, 680-690

766 Cramer, W., Kicklighter, D.W., Bondeau, A., Iii, B.M., Churkina, G., Nemry, B.,  
767 Ruimy, A., Schloss, A.L., & Intercomparison, T.P.O.F.T.P.N.M. (1999).  
768 Comparing global models of terrestrial net primary productivity (NPP): overview  
769 and key results. *Global Change Biology*, 5, 1-15

770 Curran, P.J., & Dash, J. (2005). ALGORITHM THEORETICAL BASIS DOCUMENT  
771 ATBD 2.22 CHLOROPHYLL INDEX. *University of Southampton, Southampton-*  
772 *UK*

773 Dash, J., & Curran, P.J. (2004). The MERIS terrestrial chlorophyll index.  
774 *International Journal of Remote Sensing*, 25, 5403-5413

775 Dash, J., Curran, P.J., Tallis, M.J., Llewellyn, G.M., Taylor, G., & Snoeij, P. (2010).  
776 Validating the MERIS Terrestrial Chlorophyll Index (MTCI) with ground  
777 chlorophyll content data at MERIS spatial resolution. *International Journal of*  
778 *Remote Sensing*, 31, 5513-5532

779 DeLucia, E.H., & Thomas, R.B. (2000). Photosynthetic Responses to CO<sub>2</sub>  
780 Enrichment of Four Hardwood Species in a Forest Understory. *Oecologia*, 122,  
781 11-19

782 Desanker, P.V., Frost, P.G.H., Justice, C.O., & Scholes, R.J. (1997). The Miombo  
783 Network: Framework for a terrestrial transect study of land-use and land-cover  
784 change in the miombo ecosystems of Central Africa. In, *IGBP Global change*  
785 *report: International Geosphere-Biosphere Programme*

786 Ehleringer, J., & Björkman, O. (1977). Quantum Yields for CO<sub>2</sub> Uptake in C<sub>3</sub> and  
787 C<sub>4</sub> Plants Dependence on temperature, CO<sub>2</sub>, and O<sub>2</sub> concentration. *Plant*  
788 *Physiology*, 59, 86-90

789 Ehleringer, J., & Pearcy, R.W. (1983). Variation in Quantum Yield for CO<sub>2</sub> Uptake  
790 among C<sub>3</sub> and C<sub>4</sub> Plants. *Plant Physiology*, 73, 555

791 Falge, E., Baldocchi, D., Tenhunen, J., Aubinet, M., Bakwin, P., Berbigier, P.,  
792 Bernhofer, C., Burba, G., Clement, R., Davis, K.J., Elbers, J.A., Goldstein, A.H.,  
793 Grelle, A., Granier, A., Guðmundsson, J., Hollinger, D., Kowalski, A.S., Katul,  
794 G., Law, B.E., Malhi, Y., Meyers, T., Monson, R.K., Munger, J.W., Oechel, W.,  
795 Paw U, K.T., Pilegaard, K., Rannik, Ü., Rebmann, C., Suyker, A., Valentini, R.,  
796 Wilson, K., & Wofsy, S. (2002). Seasonality of ecosystem respiration and gross  
797 primary production as derived from FLUXNET measurements. *Agricultural and*  
798 *Forest Meteorology*, 113, 53-74

799 Falge, E., Baldocchi, D., Tenhunen, J., Aubinet, M., Bakwin, P., Berbigier, P.,  
800 Bernhofer, C., Burba, G., Clement, R., Davis, K.J., Elbers, J.A., Goldstein, A.H.,  
801 Grelle, A., Granier, A., Guðmundsson, J., Hollinger, D., Kowalski, A.S., Katul,  
802 G., Law, B.E., Malhi, Y., Meyers, T., Monson, R.K., Munger, J.W., Oechel, W.,  
803 Paw U, K.T., Pilegaard, K., Rannik, Ü., Rebmann, C., Suyker, A., Valentini, R.,  
804 Wilson, K., & Wofsy, S. (2002). Seasonality of ecosystem respiration and gross  
805 primary production as derived from FLUXNET measurements. *Agricultural and*  
806 *Forest Meteorology*, 113, 53-74

807 Fattore, F., Bertolini, T., Materia, S., Gualdi, S., Thongo M'Bou, A., Nicolini, G.,  
808 Valentini, R., De Grandcourt, A., Tedesco, D., & Castaldi, S. (2014). Seasonal  
809 trends of dry and bulk concentration of nitrogen compounds over a rain forest  
810 in Ghana. *Biogeosciences*, 11, 3069-3081

811 Fensholt, R., Sandholt, I., & Rasmussen, M.S. (2004). Evaluation of MODIS LAI,  
812 fAPAR and the relation between fAPAR and NDVI in a semi-arid environment  
813 using in situ measurements. *Remote Sensing of Environment*, 91, 490-507

814 Gitelson, A.A., Peng, Y., Masek, J.G., Rundquist, D.C., Verma, S., Suyker, A.,  
815 Baker, J.M., Hatfield, J.L., & Meyers, T. (2012). Remote estimation of crop gross  
816 primary production with Landsat data. *Remote Sensing of Environment*, 121,  
817 404-414

818 Hamby, D.M. (1993). A numerical comparison of sensitivity analysis techniques.  
819 In. Westinghouse Savannah River Co., Aiken, SC (United States).

820 Hanan, N.P., Kabat, P., Dolman, A.J., & Elbers, J.A. (1998). Photosynthesis and  
821 carbon balance of a Sahelian fallow savanna. *Global Change Biology*, 4, 523-  
822 538

823 Harris, A., & Dash, J. (2010). The potential of the MERIS Terrestrial Chlorophyll  
824 Index for carbon flux estimation. *Remote Sensing of Environment*, 114, 1856-  
825 1862

826 Harris, A., & Dash, J. (2011). A new approach for estimating northern peatland  
827 gross primary productivity using a satellite-sensor-derived chlorophyll index.  
828 *Journal of Geophysical Research: Biogeosciences*, 116, n/a-n/a

829 Hilker, T., Coops, N.C., Wulder, M.A., Black, T.A., & Guy, R.D. (2008). The use of  
830 remote sensing in light use efficiency based models of gross primary production:  
831 A review of current status and future requirements. *Science of The Total*  
832 *Environment*, 404, 411-423

833 Huston, M.A., & Wolverton, S. (2009). The global distribution of net primary  
834 production: resolving the paradox. *Ecological Monographs*, 79, 343-377



835 Ibrahim, Z.Y., Balzter, H., Kaduk, J., & Tucker, J.C. (2015). Land Degradation  
836 Assessment Using Residual Trend Analysis of GIMMS NDVI3g, Soil Moisture and  
837 Rainfall in Sub-Saharan West Africa from 1982 to 2012. *Remote Sensing*, 7

838 Jarvis, P.G., & Leverenz, J.W. (1983). Productivity of Temperate, Deciduous and  
839 Evergreen Forests. In O.L. Lange, P.S. Nobel, C.B. Osmond, & H. Ziegler (Eds.),  
840 *Physiological Plant Ecology IV: Ecosystem Processes: Mineral Cycling,*  
841 *Productivity and Man's Influence* (pp. 233-280). Berlin, Heidelberg: Springer  
842 Berlin Heidelberg

843 Kicklighter, D.W., Bondeau, A., Schloss, A.L., Kaduk, J., McGuire, A.D., &  
844 Intercomparison, T.P.O.F.T.P.N.M. (1999). Comparing global models of  
845 terrestrial net primary productivity (NPP): global pattern and differentiation by  
846 major biomes. *Global Change Biology*, 5, 16-24

847 Kim, D., Oren, R., & Qian, S.S. (2016). Response to CO2 enrichment of understory  
848 vegetation in the shade of forests. *Global Change Biology*, 22, 944-956

849 Li, W., Weiss, M., Waldner, F., Defourny, P., Demarez, V., Morin, D., Hagolle, O.,  
850 & Baret, F. (2015). A Generic Algorithm to Estimate LAI, FAPAR and FCOVER  
851 Variables from SPOT4\_HRVIR and Landsat Sensors: Evaluation of the  
852 Consistency and Comparison with Ground Measurements. *Remote Sensing*, 7

853 Liang, S., & Zhang, X. (2012). Global Land Surface Products: Photosynthetically  
854 Active Radiation Data Collection(2008-2010). In: Beijing Normal University.

855 Liang, S., Zheng, T., Liu, R., Fang, H., Tsay, S.-C., & Running, S. (2006).  
856 Estimation of incident photosynthetically active radiation from Moderate  
857 Resolution Imaging Spectrometer data. *Journal of Geophysical Research:*  
858 *Atmospheres*, 111, n/a-n/a

Formatted: German (Germany)

859 McCallum, I., Franklin, O., Moltchanova, E., Merbold, L., Schmulius, C., Shvidenko,  
860 A., Schepaschenko, D., & Fritz, S. (2013). Improved light and temperature  
861 responses for light-use-efficiency-based GPP models. *Biogeosciences*, *10*,  
862 6577-6590

863 Merbold, L., Ardö, J., Arneth, A., Scholes, R.J., Nouvellon, Y., de Grandcourt, A.,  
864 Archibald, S., Bonnefond, J.M., Boulain, N., Brueggemann, N., Bruemmer, C.,  
865 Cappelaere, B., Ceschia, E., El-Khidir, H.A.M., El-Tahir, B.A., Falk, U., Lloyd, J.,  
866 Kergoat, L., Le Dantec, V., Mougou, E., Muchinda, M., Mukelabai, M.M., Ramier,  
867 D., Roupsard, O., Timouk, F., Veenendaal, E.M., & Kutsch, W.L. (2009).  
868 Precipitation as driver of carbon fluxes in 11 African ecosystems. *Biogeosciences*,  
869 *6*, 1027-1041

870 Monteith, J.L. (1972). Solar radiation and productivity in tropical ecosystems.  
871 *Journal of applied ecology*, *9*, 747-766

872 Myneni, R.B., & Williams, D.L. (1994). On the relationship between FAPAR and  
873 NDVI. *Remote Sensing of Environment*, *49*, 200-211

874 Ogutu, B.O., & Dash, J. (2013). An algorithm to derive the fraction of  
875 photosynthetically active radiation absorbed by photosynthetic elements of the  
876 canopy (FAPARps) from eddy covariance flux tower data. *New Phytologist*, *197*,  
877 511-523

878 Ogutu, B.O., Dash, J., & Dawson, T.P. (2013). Developing a diagnostic model for  
879 estimating terrestrial vegetation gross primary productivity using the  
880 photosynthetic quantum yield and Earth Observation data. *Global Change*  
881 *Biology*, *19*, 2878-2892

882 Papale, D., Reichstein, M., Aubinet, M., Canfora, E., Bernhofer, C., Kutsch, W.,  
883 Longdoz, B., Rambal, S., Valentini, R., Vesala, T., & Yakir, D. (2006). Towards  
884 a standardized processing of Net Ecosystem Exchange measured with eddy  
885 covariance technique: algorithms and uncertainty estimation. *Biogeosciences*,  
886 3, 571-583

887 Ran, Y., Li, X., Sun, R., Kljun, N., Zhang, L., Wang, X., & Zhu, G. (2016). Spatial  
888 representativeness and uncertainty of eddy covariance carbon flux  
889 measurements for upscaling net ecosystem productivity to the grid scale.  
890 *Agricultural and Forest Meteorology*, 230, 114-127

Formatted: German (Germany)

891 Ruimy, A., Kergoat, L., Bondeau, A., & Intercomparison, T.P.O.F.T.P.N.M. (1999).  
892 Comparing global models of terrestrial net primary productivity (NPP): analysis  
893 of differences in light absorption and light-use efficiency. *Global Change Biology*,  
894 5, 56-64

895 Scholes, R.J., Frost, P.G.H., & Tian, Y. (2004). Canopy structure in savannas along  
896 a moisture gradient on Kalahari sands. *Global Change Biology*, 10, 292-302

897 Sims, D.A., Rahman, A.F., Cordova, V.D., El-Masri, B.Z., Baldocchi, D.D.,  
898 Flanagan, L.B., Goldstein, A.H., Hollinger, D.Y., Misson, L., Monson, R.K.,  
899 Oechel, W.C., Schmid, H.P., Wofsy, S.C., & Xu, L. (2006). On the use of MODIS  
900 EVI to assess gross primary productivity of North American ecosystems. *Journal*  
901 *of Geophysical Research: Biogeosciences*, 111, n/a-n/a

902 Singaas, E.L., Ort, D.R., & DeLucia, E.H. (2001). Variation in measured values of  
903 photosynthetic quantum yield in ecophysiological studies. *Oecologia*, 128, 15-  
904 23

905 Sjöström, M., Ardö, J., Arneth, A., Boulain, N., Cappelaere, B., Eklundh, L., de  
906 Grandcourt, A., Kutsch, W.L., Merbold, L., Nouvellon, Y., Scholes, R.J., Schubert,  
907 P., Seaquist, J., & Veenendaal, E.M. (2011). Exploring the potential of MODIS  
908 EVI for modeling gross primary production across African ecosystems. *Remote*  
909 *Sensing of Environment*, 115, 1081-1089

910 Sjöström, M., Zhao, M., Archibald, S., Arneth, A., Cappelaere, B., Falk, U., de  
911 Grandcourt, A., Hanan, N., Kergoat, L., Kutsch, W., Merbold, L., Mougin, E.,  
912 Nickless, A., Nouvellon, Y., Scholes, R.J., Veenendaal, E.M., & Ardö, J. (2013).  
913 Evaluation of MODIS gross primary productivity for Africa using eddy covariance  
914 data. *Remote Sensing of Environment*, 131, 275-286

915 Suyker, A.E., & Verma, S.B. (2010). Coupling of carbon dioxide and water vapor  
916 exchanges of irrigated and rainfed maize–soybean cropping systems and water  
917 productivity. *Agricultural and Forest Meteorology*, 150, 553-563

918 Suyker, A.E., & Verma, S.B. (2012). Gross primary production and ecosystem  
919 respiration of irrigated and rainfed maize–soybean cropping systems over 8  
920 years. *Agricultural and Forest Meteorology*, 165, 12-24

921 Svoray, T., & Karnieli, A. (2011). Rainfall, topography and primary production  
922 relationships in a semiarid ecosystem. *Ecohydrology*, 4, 56-66

923 Tu, K. (2000). Modeling plant-soil-atmosphere carbon dioxide exchange using  
924 optimality principles. PhD Thesis; University of New Hampshire

925 Turner, D.P., Ritts, W.D., Cohen, W.B., Gower, S.T., Zhao, M., Running, S.W.,  
926 Wofsy, S.C., Urbanski, S., Dunn, A.L., & Munger, J.W. (2003). Scaling Gross  
927 Primary Production (GPP) over boreal and deciduous forest landscapes in

928 support of MODIS GPP product validation. *Remote Sensing of Environment*, 88,  
929 256-270

930 Unwin, D.M. (1980). *Microclimate measurement for ecologists*. Academic Press  
931 Inc.

932 Valentini, R., Arneeth, A., Bombelli, A., Castaldi, S., Cazzolla Gatti, R., Chevallier,  
933 F., Ciais, P., Grieco, E., Hartmann, J., Henry, M., Houghton, R.A., Jung, M.,  
934 Kutsch, W.L., Malhi, Y., Mayorga, E., Merbold, L., Murray-Tortarolo, G., Papale,  
935 D., Peylin, P., Poulter, B., Raymond, P.A., Santini, M., Sitch, S., Vaglio Laurin,  
936 G., van der Werf, G.R., Williams, C.A., & Scholes, R.J. (2014). A full greenhouse  
937 gases budget of Africa: synthesis, uncertainties, and vulnerabilities.  
938 *Biogeosciences*, 11, 381-407

939 Verma, S.B., Dobermann, A., Cassman, K.G., Walters, D.T., Knops, J.M.,  
940 Arkebauer, T.J., Suyker, A.E., Burba, G.G., Amos, B., Yang, H., Ginting, D.,  
941 Hubbard, K.G., Gitelson, A.A., & Walter-Shea, E.A. (2005). Annual carbon  
942 dioxide exchange in irrigated and rainfed maize-based agroecosystems.  
943 *Agricultural and Forest Meteorology*, 131, 77-96

944 Veroustraete, F., Sabbe, H., & Eerens, H. (2002). Estimation of carbon mass fluxes  
945 over Europe using the C-Fix model and Euroflux data. *Remote Sensing of*  
946 *Environment*, 83, 376-399

947 Walker, B.H. (1987). *Determinants of tropical savannas*. Published by IRL Press  
948 on behalf of the ICSU Press for the International Union of Biological Sciences

949 Weber, U., Jung, M., Reichstein, M., Beer, C., Braakhekke, M.C., Lehsten, V.,  
950 Ghent, D., Kaduk, J., Viovy, N., Ciais, P., Gobron, N., & Rödenbeck, C. (2009).

951 The interannual variability of Africa's ecosystem productivity: a multi-model  
952 analysis. *Biogeosciences*, 6, 285-295

953 Williams, C.A., Hanan, N.P., Neff, J.C., Scholes, R.J., Berry, J.A., Denning, A.S., &  
954 Baker, D.F. (2007). Africa and the global carbon cycle. *Carbon Balance and*  
955 *Management*, 2, 3

956 Williams, J.W., & Jackson, S.T. (2007). Novel climates, no-analog communities,  
957 and ecological surprises. *Frontiers in Ecology and the Environment*, 5, 475-482

958 Wu, C., Munger, J.W., Niu, Z., & Kuang, D. (2010). Comparison of multiple models  
959 for estimating gross primary production using MODIS and eddy covariance data  
960 in Harvard Forest. *Remote Sensing of Environment*, 114, 2925-2939

961 Wu, C., Niu, Z., Tang, Q., Huang, W., Rivard, B., & Feng, J. (2009). Remote  
962 estimation of gross primary production in wheat using chlorophyll-related  
963 vegetation indices. *Agricultural and Forest Meteorology*, 149, 1015-1021

964 Zhang, Q., Cheng, Y.-B., Lyapustin, A.I., Wang, Y., Gao, F., Suyker, A., Verma,  
965 S., & Middleton, E.M. (2014). Estimation of crop gross primary production (GPP):  
966 fAPARchl versus MOD15A2 FPAR. *Remote Sensing of Environment*, 153, 1-6

967 Zhang, Q., Middleton, E.M., Cheng, Y.-B., Huemmrich, K.F., Cook, B.D., Corp, L.A.,  
968 Kustas, W.P., Russ, A.L., Prueger, J.H., & Yao, T. (2016). Integrating chlorophyll  
969 fAPAR and nadir photochemical reflectance index from EO-1/Hyperion to predict  
970 cornfield daily gross primary production. *Remote Sensing of Environment*, 186,  
971 311-321

972 Zhang, Q., Middleton, E.M., Gao, B.C., & Cheng, Y.B. (2012). Using EO-1 Hyperion  
973 to Simulate HypsIRI Products for a Coniferous Forest: The Fraction of PAR

974 Absorbed by Chlorophyll (FAPAR<sub>chl</sub>) and Leaf Water Content (LWC). *IEEE*  
975 *Transactions on Geoscience and Remote Sensing*, 50, 1844-1852

976 Zhang, Y., Xu, M., Chen, H., & Adams, J. (2009). Global pattern of NPP to GPP  
977 ratio derived from MODIS data: effects of ecosystem type, geographical location  
978 and climate. *Global Ecology and Biogeography*, 18, 280-290

979